nature neuroscience

Sparse, decorrelated odor coding in the mushroom body enhances learned odor discrimination

Andrew C Lin[1], Alexei M Bygrave[1], Alix de Calignon[1], Tzumin Lee[2] & Gero Miesenböck[1]

Sparse coding may be a general strategy of neural systems for augmenting memory capacity. In *Drosophila melanogaster*, sparse odor coding by the Kenyon cells of the mushroom body is thought to generate a large number of precisely addressable locations for the storage of odor-specific memories. However, it remains untested how sparse coding relates to behavioral performance. Here we demonstrate that sparseness is controlled by a negative feedback circuit between Kenyon cells and the GABAergic anterior paired lateral (APL) neuron. Systematic activation and blockade of each leg of this feedback circuit showed that Kenyon cells activated APL and APL inhibited Kenyon cells. Disrupting the Kenyon cell–APL feedback loop decreased the sparseness of Kenyon cell odor responses, increased inter-odor correlations and prevented flies from learning to discriminate similar, but not dissimilar, odors. These results suggest that feedback inhibition suppresses Kenyon cell activity to maintain sparse, decorrelated odor coding and thus the odor specificity of memories.

To adapt to their environments, animals must learn which stimuli are associated with positive or negative outcomes and distinguish these stimuli from similar but irrelevant ones. One widely proposed mechanism for implementing stimulus-specific associative memories is sparse coding, in which only a few neurons out of a population respond to any given stimulus and each neuron responds to only a few stimuli out of all possible stimuli. Theoretical work has suggested that sparse coding increases the capacity of associative memory by reducing overlap between representations[1–4]. Experimentally, sparse representations of sensory information have been observed in many systems, including vision[5], audition[6], touch[7] and olfaction[8–12]. However, despite the accumulating evidence for widespread sparse coding and theoretical arguments for its importance, a demonstration that sparse coding improves the stimulus specificity of associative memory has been lacking. Addressing this gap experimentally must begin with an understanding of how sparse coding arises, a problem that also remains incompletely understood (but see refs. 8,13–16).

An attractive model for studying these questions is the *Drosophila* olfactory system. Projection neurons (PNs), the second-order neurons that carry olfactory information from the antennal lobe to the protocerebrum, encode odors broadly: many PNs respond to the majority of odor stimuli, and many odors elicit responses in most PNs, in both locust and *Drosophila*[8,17]. This odor code is dramatically sparsened at the third level of olfactory processing, the Kenyon cells of the mushroom body, where, in both locust and *Drosophila*, only ~5–10% of Kenyon cells respond to any given odor, and Kenyon cells that do respond fire only a few spikes[8,9,12,18]. Notably, Kenyon cells are the main site of olfactory associative memory storage[19]. The sparseness of Kenyon cell activity may reduce overlap between odor representations and thereby help the animal retrieve distinct learned responses to similar odors[13,14].

The low activity levels associated with sparse coding suggest a role for inhibition. Indeed, feedforward and feedback inhibitory motifs are common in sparsely responding sensory systems and have been widely suggested to underlie sparseness[11,15,16,20,21]. However, direct evidence that inhibition causes sparseness and that sparseness is behaviorally relevant is scant. The ability in *Drosophila* to combine optical imaging of neuronal population responses[12,22], acute silencing[23] and activation[24,25] of genetically defined neurons, and behavioral assays for learned odor discrimination[26,27] provides a unique opportunity to test the hypotheses that (i) feedback inhibition underlies sparse odor coding in Kenyon cells and (ii) sparse odor coding improves the stimulus specificity of associative memory.

RESULTS

Feedback inhibition of Kenyon cell responses

To test whether Kenyon cell activity leads to negative feedback onto Kenyon cells themselves, we acutely blocked Kenyon cell synaptic output using temperature-sensitive shibire (shi^{ts1}), a dominant-negative mutant of dynamin that interferes with synaptic vesicle re-endocytosis at the restrictive temperature[23] (>30 °C). We took advantage of the fact that shi^{ts1} blocks synaptic transmission, not electrical activity, by coexpressing shi^{ts1} and the Ca^{2+} reporter GCaMP3 in Kenyon cells.

Control flies expressing only GCaMP3 under the control of *mb247-LexA* showed robust odor-evoked Ca^{2+} influx in the α lobe that did not change, or decreased slightly, at the restrictive 32 °C compared to the permissive 22 °C (**Fig. 1a**). In contrast, flies expressing both GCaMP3 and shi^{ts1} in Kenyon cells exhibited greatly increased odor-evoked Ca^{2+} transients at 32 °C (**Fig. 1b**). The odor response recovered to baseline upon return to 22 °C in most but not all cases, consistent with previous reports that recovery from shi^{ts1} inactivation is not always complete[28]. The significant temperature

[1]Centre for Neural Circuits and Behaviour, University of Oxford, Oxford, UK. [2]Janelia Farm Research Campus, Howard Hughes Medical Institute, Ashburn, Virginia, USA. Correspondence should be addressed to G.M. (gero.miesenboeck@cncb.ox.ac.uk).

Received 6 November 2013; accepted 23 January 2014; published online 23 February 2014; doi:10.1038/nn.3660

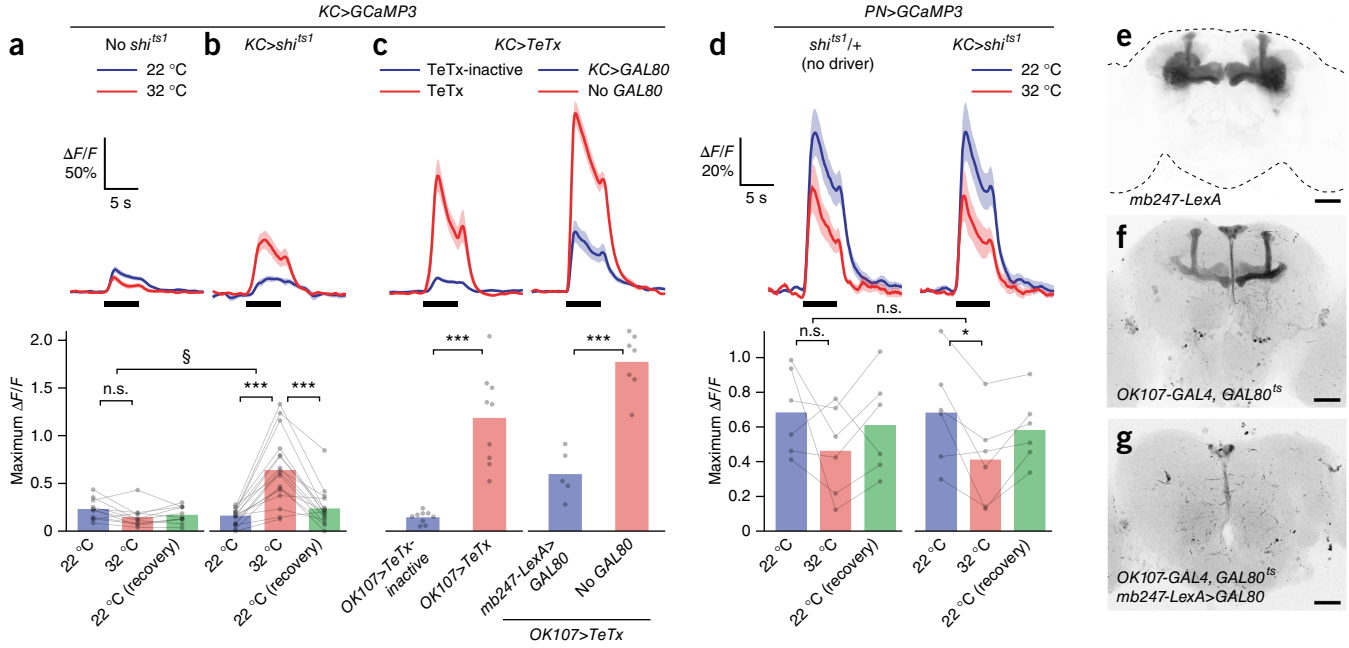

Figure 1 Feedback inhibition of Kenyon cell responses by Kenyon cell output. (**a**) Kenyon cells in control *mb247-LexA>GCaMP3* flies showed no temperature-dependent increase in odor-evoked Ca^{2+} influx in the α lobe. Black bars, 5-s pulses of ethyl acetate. Traces, average Δ*F*/*F* (fluorescence change normalized to baseline); shading, s.e.m. $n = 11$ [10] (number of brain hemispheres [number of flies]). n.s., $P = 0.06$, repeated-measures ANOVA with Geisser-Greenhouse correction and Holm-Sidak multiple comparisons test. (**b**) Kenyon cells in experimental *mb247-LexA>GCaMP3,shi^ts1* flies showed a large temperature-dependent increase in odor-evoked Ca^{2+} influx in the α lobe. $n = 16$ [15]. $^{***}P < 0.001$, Friedman test with Dunn's multiple comparisons test. §$P < 0.001$, Mann-Whitney *U*-test, comparing ratios of odor-evoked Ca^{2+} influx at 32 °C versus 22 °C between control and *mb247-LexA>GCaMP3,shi^ts1* flies. (**c**) Left panels: *OK107>TeTx* flies (red, $n = 9$) showed a large increase in odor-evoked Ca^{2+} influx in the α lobe as compared to *OK107>TeTx-inactive* flies (blue, $n = 9$). Right panels: odor-evoked Ca^{2+} influx was higher in *OK107>TeTx, mb247-LexA>GCaMP3* flies (blue, $n = 5$) than in *OK107>TeTx, mb247-LexA>GCaMP3,GAL80* flies (red, $n = 7$). $^{***}P < 0.001$, unpaired Welch *t*-test. (**d**) Odor-evoked Ca^{2+} influx in PNs innervating the calyx declined slightly with temperature in both *NP225>GCaMP3, mb247-LexA>shi^ts1* ($P = 0.04$) and *NP225>GCaMP3, shi^ts1/+* flies (n.s., $P = 0.27$). $^{*}P = 0.04$, repeated-measures ANOVA with Geisser-Greenhouse correction and Holm-Sidak multiple comparisons test. $n = 6$. The ratio of odor-evoked Ca^{2+} influx at 32 °C versus 22 °C did not differ significantly between left and right panels (n.s., $P = 0.60$, unpaired Welch *t*-test). (**e**–**g**) Representative maximum intensity projections of confocal image stacks showing expression patterns of *mb247-LexA* (**e**), *OK107, GAL80^ts* (**f**) and *OK107, GAL80^ts, mb247-LexA>Gal80* (**g**). Dashed lines show the outline of the brain. Scale bars, 50 μm. See **Supplementary Table 1** for full genotypes.

effect in flies expressing GCaMP3 and shi^{ts1} compared to flies expressing only GCaMP3 (**Fig. 1a**,**b**) is unlikely to be caused by blocking neurons other than Kenyon cells because *mb247-LexA* shows little or no expression elsewhere (**Fig. 1e**).

To eliminate the possibility that shi^{ts1} inactivation affects synaptic integration by preventing membrane retrieval and thereby increasing membrane capacitance, we used tetanus toxin light chain (TeTx), which blocks vesicle exo- rather than endocytosis[29]. We targeted TeTx to Kenyon cells with the help of *OK107-GAL4* and used *tubP-GAL80^ts* to suppress transgene expression during development. Inactivation of the $GAL80^{ts}$ repressor by heating <1-d-old flies to 31 °C for 16–24 h induced transgene expression in the pattern previously reported[30] for *OK107-GAL4* (**Fig. 1f**). Acute expression of TeTx led to increased odor-evoked Ca^{2+} influx relative to that seen upon acute expression of a catalytically inactive toxin[29] (**Fig. 1c**). The effect was abolished by *mb247-LexA*-driven expression of GAL80 (**Fig. 1c**), which subtracts Kenyon cells from the *OK107-GAL4* pattern (**Fig. 1g**). Together, these results suggest that feedback inhibition suppresses Kenyon cell responses.

In *Drosophila*, Kenyon cells have been proposed to communicate with the antennal lobe via unidentified cholinergic neurons[31], while in mammals, feedback from the olfactory cortex inhibits the mitral cells of the olfactory bulb[32,33]. We therefore examined whether the Kenyon cell–driven inhibitory feedback operates directly on Kenyon cells or an earlier stage of the olfactory pathway, by expressing GCaMP3 under *NP225-GAL4* control in PNs. Odor-evoked responses of PNs innervating the mushroom body calyx did not increase after the removal of Kenyon cell output in *PN>GCaMP3, KC>shi^ts1* flies (**Fig. 1d**). Indeed, PN odor responses in both *lexAop-shi^ts1*; *mb247-LexA* and *lexAop-shi^ts1*/+ flies decreased slightly at the elevated temperature, but there was no difference in the magnitude of the decrease between the two groups (**Fig. 1d**). The small temperature effect was therefore unrelated to shi^{ts1}-mediated blockade of Kenyon cells. These results indicate that feedback inhibition operates directly on the mushroom body.

Feedback is from all Kenyon cells to all Kenyon cells

Kenyon cells are subdivided into three main classes: γ neurons project to the horizontal lobes only, while the axons of αβ and α′β′ neurons bifurcate to form the α and α′ portions of the vertical lobes and the β and β′ portions of the horizontal lobes (**Fig. 2**). If feedback inhibition were strictly local or Kenyon cell class–specific, blocking output from one class would increase odor responses only in those cells. In contrast, if feedback were all-to-all, blockade of one class of Kenyon cells would have little effect because of compensatory drive from other Kenyon cells. To distinguish between these possibilities, we separately blocked the synaptic output of each main class of Kenyon cells, driving shi^{ts1} in αβ neurons using *c739-GAL4*, in α′β′ neurons using *R35B12-GAL4* and in γ neurons using *R64C08-GAL4* (**Supplementary Fig. 1**), while imaging odor responses in all lobes.

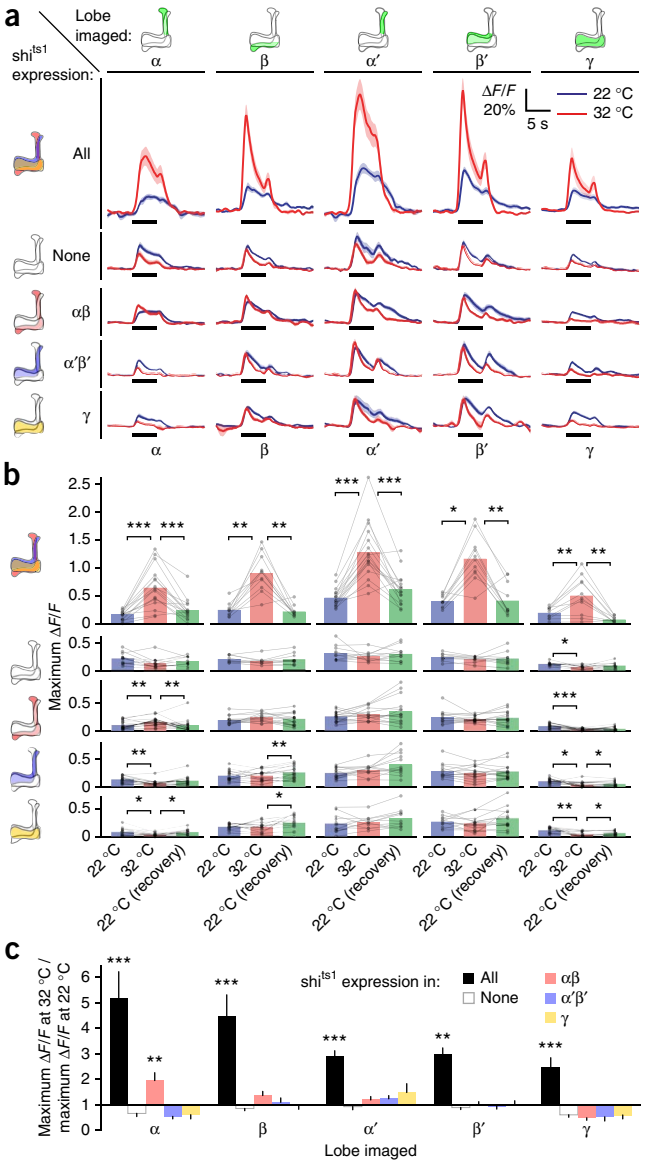

Figure 2 Feedback is from all Kenyon cells to all Kenyon cells. (**a**) Effect of blocking output of different Kenyon cell populations (rows) on odor-evoked Ca^{2+} influx in different mushroom body lobes (columns). Blocking all Kenyon cells increased odor-evoked Ca^{2+} influx in all lobes of the mushroom body in *mb247-LexA>GCaMP3,shi^{ts1}* flies. Raising the temperature had no effect on, or slightly decreased, odor responses in all lobes of control *mb247-LexA>GCaMP3* flies. Blocking αβ neurons slightly increased odor responses only in the α lobes of *mb247-LexA>GCaMP3, c739>shi^{ts1}* flies. Blocking α′β′ neurons did not affect odor responses in *mb247-LexA>GCaMP3, R35B12>shi^{ts1}* flies. Blocking γ neurons did not affect odor responses in *mb247-LexA>GCaMP3, R64C08>shi^{ts1}* flies. (**b**) Summary of data from **a**. *n*, left to right, given as number of brain hemispheres [number of flies]: All: 16 [15], 11 [6], 17 [16], 11 [6], 11 [6]. None: 11 [10], 9 [7], 11 [10], 9 [7], 9 [7]. αβ: 16 [9], 15 [8], 16 [9], 15 [8], 15 [8]. α′β′: 13 [8] (all). γ: 11 [6] (all). $*P < 0.05$, $**P < 0.01$, $***P < 0.001$, repeated-measures ANOVA with Geisser-Greenhouse correction and Holm-Sidak multiple comparisons test or Friedman test with Dunn's multiple comparisons test, as appropriate. (**c**) Ratios of odor-evoked Ca^{2+} influx at 32 °C versus 22 °C for data in **a**,**b**. $**P < 0.01$, $***P < 0.001$, Kruskal-Wallis ANOVA with *post hoc* Mann-Whitney *U*-tests using Holm-Bonferroni multiple comparisons correction. Error bars, s.e.m. See **Supplementary Table 1** for full genotypes.

Blocking the output of all Kenyon cells in *lexAop-shi^{ts1}*; *mb247-LexA* flies increased odor responses throughout the mushroom body (**Fig. 2**). In contrast, blocking only αβ Kenyon cells slightly elevated the odor responses of these cells but left those of other Kenyon cells unaltered; the increase of αβ responses, however, was minuscule compared to that observed in the same neurons after blocking output from all Kenyon cells (**Fig. 2**). Blocking only α′β′ or only γ neurons had no effect on odor responses in any lobe (**Fig. 2**). Similar results were seen with the α′β′ driver *c305a-GAL4* and the γ drivers *NP1131-GAL4*, *H24-GAL4* and *1471-GAL4* (data not shown). Because blocking output from all Kenyon cells is required to suppress inhibition in any lobe, feedback is in all likelihood all-to-all. The subtly different consequences of blocking αβ versus α′β′ versus γ neurons may simply reflect the differing sizes of these neuronal populations (about one-half, one-sixth and one-third of all Kenyon cells, respectively[30]).

Kenyon cells activate APL

All-to-all feedback suggests that Kenyon cell output is integrated into a single inhibitory feedback signal, perhaps by a single neuron. In locust, a giant GABAergic neuron (GGN) present in a single copy per hemisphere provides negative feedback to Kenyon cells[15]. The GGN is most likely the locust analog of the *Drosophila* anterior paired lateral (APL) neuron. Each hemisphere of the *Drosophila* brain contains one APL neuron, which extends processes throughout the calyx, peduncle and lobes of the mushroom body[34,35]. The APL neuron is GABAergic and responds to odors with depolarization and Ca^{2+} influx[15,34]. Kenyon cells express the $GABA_A$ receptor RDL, and overexpression of RDL reduces the amplitude of Kenyon cell odor-evoked Ca^{2+} influx, while knockdown of RDL by RNA interference (RNAi) increases it[36]. As in locust[15], where Kenyon cell spikes elicit excitatory postsynaptic potentials in the GGN, the APL neuron might thus form a negative feedback loop with Kenyon cells.

To probe for connectivity between APL and Kenyon cells, we expressed *lexAop-dTRPA1* under *mb247-LexA* control in Kenyon cells and imaged calcium transients or synaptic vesicle release[22] in APL, using *UAS-GCaMP3* or *UAS-synapto-pHluorin* (spH) driven by *GH146-GAL4*. *dTRPA1* encodes a cation channel whose conductance gates open at elevated temperatures (>25 °C), stimulating activity[25]. Thermal activation of Kenyon cells caused large increases in GCaMP3 and spH signals emitted by APL projections in the vertical mushroom body lobes (**Fig. 3a**,**b**). The signals were absent in flies carrying the *lexAop-dTRPA1* responder but lacking the *mb247-LexA* driver transgene (**Fig. 3c**,**d**). These results, together with the anatomy of the APL neuron[34,35], suggest that the APL odor response is driven by Kenyon cells. The response should therefore vanish when Kenyon cell output is blocked. Indeed, in flies expressing *mb247-LexA*-driven shi^{ts1}, but not in *lexAop-shi^{ts1}*/+ controls lacking the *mb247-LexA* driver, odor-evoked GCaMP3 responses were blocked at the restrictive temperature and restored at the permissive temperature (**Fig. 3e**). Although these data do not distinguish between a direct (monosynaptic) and an indirect connection between Kenyon cells and APL, they do identify Kenyon cells as the source of odor input to APL, thus delineating one leg of the negative feedback loop.

APL inhibits Kenyon cells

While the odor-evoked Ca^{2+} transients in APL branches innervating the mushroom body might reflect postsynaptic activity only, the spH signal indicates that APL also forms presynaptic specializations in the lobes that release transmitter in response to odors. We therefore asked whether Kenyon cells themselves are the targets of APL inhibition. This question has been difficult to address because of a lack of clean

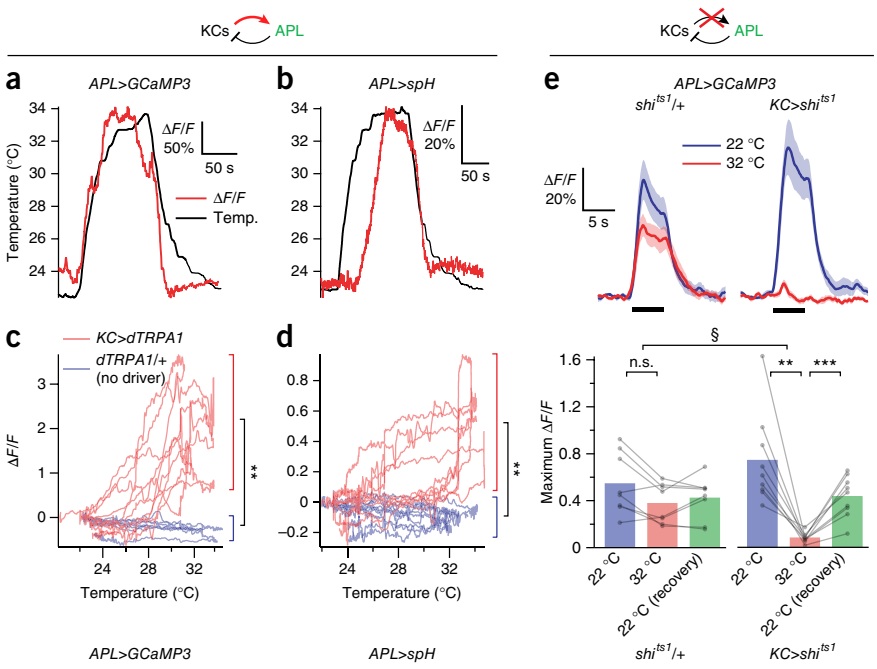

Figure 3 Kenyon cells activate APL. (**a**,**b**) Thermal activation of Kenyon cells induces Ca^{2+} influx into APL in *GH146>GCaMP3, mb247-LexA>dTRPA1* flies (**a**) and synaptic vesicle release from APL in *GH146>spH, mb247-LexA>dTRPA1* flies (**b**). Temp., temperature. (**c**,**d**) $\Delta F/F$ of GCaMP3 (**c**) and spH (**d**) as functions of temperature; each trace represents one fly. Each red trace forms a loop: in *mb247-LexA>dTRPA1* flies, $\Delta F/F$ rises as the fly is heated and falls along a different trajectory as the fly is cooled ($n = 5$). Heat did not induce Ca^{2+} influx in *GH146>GCaMP3, dTRPA1/+* flies or vesicle fusion in *GH146>spH, dTRPA1/+* flies (blue traces; GCaMP3, $n = 4$; spH, $n = 5$). $^{**}P < 0.01$, unpaired Welch *t*-test, comparing the maximum $\Delta F/F$ (between 30 °C and the temperature maximum) between *mb247-LexA>dTRPA1* and control flies. Mean ± s.e.m.: *GCaMP3, mb247-LexA>dTRPA1*, 1.90 ± 0.44; *GCaMP3, dTRPA1/+*, −0.27 ± 0.05; *spH, mb247-LexA>dTRPA1*, 0.68 ± 0.09; *spH, dTRPA1/+*, 0.06 ± 0.007. (**e**) Temperature block of transmission from Kenyon cells blocked odor-evoked APL responses in *GH146>GCaMP3, mb247-LexA>shi^{ts1}* flies (right) but not in *GH146>GCaMP3, shi^{ts1}/+* flies (left). n.s., $P = 0.07$; $^{**}P < 0.01$; $^{***}P < 0.001$; repeated-measures ANOVA with Geisser-Greenhouse correction and Holm-Sidak multiple comparisons test. $n = 8, 9$. §$P < 0.01$, Mann-Whitney *U*-test comparing ratios of odor-evoked Ca^{2+} influx at 32 °C versus 22 °C between control and *mb247-LexA>shi^{ts1}* flies. Black bars, 5-s pulses of ethyl acetate; shading, s.e.m. Schematics at top indicate which neurons were being imaged (green) and which connection was being manipulated (red arrow for dTRPA1 activation, red X for shi^{ts1} blockade). KCs, Kenyon cells. See **Supplementary Table 1** for full genotypes.

genetic access to APL[34,35]. Previous studies observed phenotypes after RNAi knockdown of the GABA biosynthetic enzyme glutamic acid decarboxylase (GAD) using *GH146-GAL4* or *NP2631-GAL4*, broad drivers that include APL[34,37,38]. However, in these approaches non-APL neurons may also be affected: *GH146-GAL4* marks ~60% of PNs, of which six neurons are GABAergic[39], while *NP2631-GAL4* is similarly broad[35]. In addition, *GAD^{RNAi}*-based knockdown of GABA release is most likely incomplete, a problem that may be compounded by homeostatic adaptation or negative feedback (see below).

To achieve specific genetic access to APL, we intersected the expression domains of *NP2631-GAL4* and *GH146-Flp*, using Flp-mediated recombination of *FRT* sites in a *tubP-FRT-GAL80-FRT* cassette (see Online Methods). Because the excision of *GAL80* by Flp recombinase is stochastic, this strategy generated flies with neither, one or both APL neurons labeled (**Fig. 4a–c** and **Supplementary Fig. 2**). We detected recombination events in APL by immunolabeling or coexpression of fluorescent proteins. Notably, we did not observe transgene expression in any neurons other than APL.

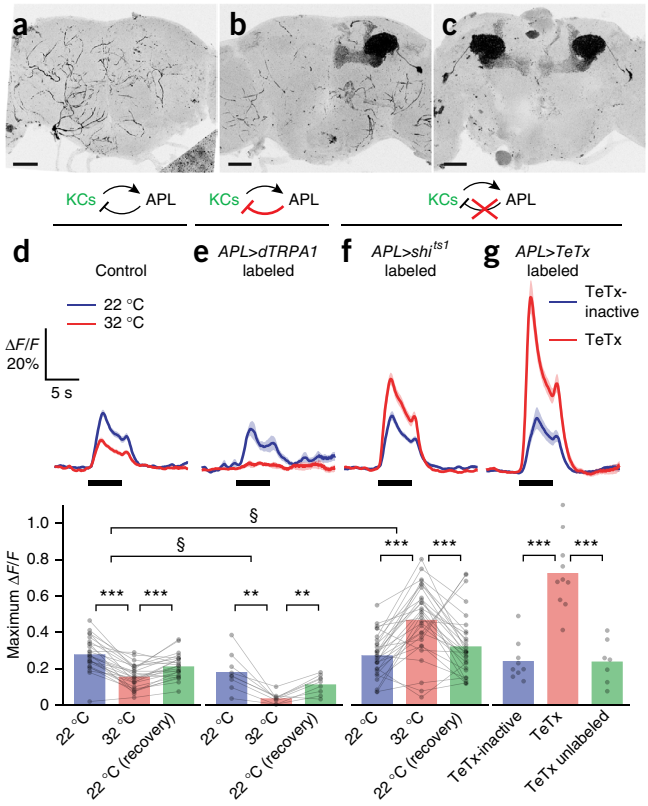

Figure 4 APL inhibits Kenyon cells. (**a**–**c**) Stochastic transgene expression in neither (**a**), one (**b**) or both (**c**) APL neurons. Scale bars, 50 µm. (**d**–**g**) Effect of different APL manipulations on odor-evoked Ca^{2+} influx in the α lobe (see **Supplementary Fig. 3** for all lobes). Black bars, 5-s pulses of ethyl acetate; shading, s.e.m. (**d**) In control hemispheres of *APL>shi^{ts1}* flies where APL was unlabeled, odor-evoked Ca^{2+} influx in Kenyon cells declined slightly at 32 °C. (**e**) In hemispheres of *APL>dTRPA1* flies where APL was labeled, odor-evoked Ca^{2+} influx in Kenyon cells was almost completely abolished at 32 °C. (**f**) In hemispheres of *APL>shi^{ts1}* flies where APL was labeled, odor-evoked Ca^{2+} influx in Kenyon cells increased greatly at 32 °C. (**g**) In APL-labeled hemispheres of *APL>TeTx* flies (red), odor-evoked Ca^{2+} influx in Kenyon cells was much higher than in APL-labeled hemispheres of *APL>TeTx-inactive* flies (blue) and APL-unlabeled hemispheres of *APL>TeTx* flies (green, lower panel). *n*, left to right, given as number of brain hemispheres [number of flies]: (**d**) $n = 24$ [17]. (**e**) $n = 9$ [5]. (**f**) $n = 30$ [21]. (**g**) $n = 9$ [7], 10 [8], 7 [6]. $^{**}P < 0.01$, $^{***}P < 0.001$, repeated-measures ANOVA with Geisser-Greenhouse correction and Holm-Sidak multiple comparisons test (**d**,**e**), Friedman test with Dunn's multiple comparisons test (**f**) or one-way ANOVA with Tukey-Kramer *post hoc* test (**g**). §$P < 0.001$, Mann-Whitney *U*-test, comparing ratios of odor-evoked Ca^{2+} influx at 32 °C versus 22 °C. See **Supplementary Table 1** for full genotypes.

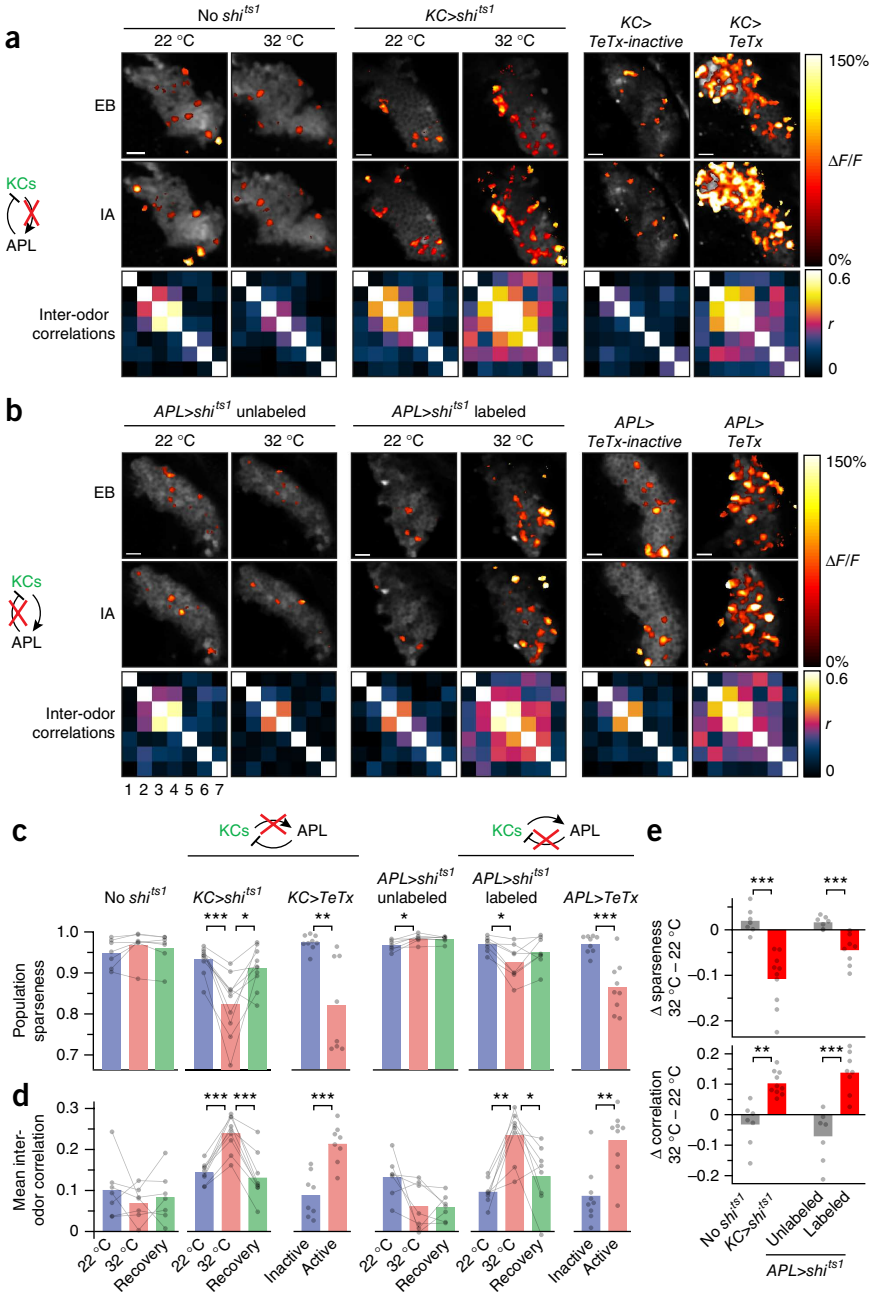

Figure 5 Inhibition keeps Kenyon cell responses sparse and distinct. (**a**,**b**) Pseudocolored activity maps of odor responses in Kenyon cell somata, overlaid on grayscale images of baseline fluorescence. Color-coded matrices represent pairwise correlations between response maps to seven odors: (1) ethyl acetate, (2) OCT, (3) butyl acetate, (4) IA, (5) EB, (6) 2-pentanol and (7) MCH. Scale bars, 10 µm. (**a**) Left: *mb247-LexA>GCaMP3*, at 22 °C and 32 °C. Center: *mb247-LexA>GCaMP3,shi^{ts1}*, at 22 °C and 32 °C. Right: *OK107>TeTx-inactive* and *OK107>TeTx*. (**b**) Left: *APL>shi^{ts1}*, APL unlabeled, at 22 °C and 32 °C. Center: *APL>shi^{ts1}*, APL labeled, at 22 °C and 32 °C. Right: *APL>TeTx-inactive* and *APL>TeTx*, APL labeled. (**c**) Population sparseness in **a**,**b** decreased when Kenyon cell or APL synaptic output was blocked. (**d**) Mean inter-odor correlations in **a**,**b** increased when Kenyon cell or APL synaptic output was blocked. *n*, left to right, given as number of brain hemispheres [number of flies]: 7, 9, 9, 8, 7 [7], 8 [7], 9 [7], 9 [7]. Schematics indicate which neurons were being imaged (green) and which connection was being manipulated (red X indicates shi^{ts1} blockade). (**e**) Temperature-dependent changes in sparseness and correlation differed between *mb247-LexA>GCaMP3* and *mb247-LexA>GCaMP3,shi^{ts1}* flies (left) and between APL-unlabeled and APL-labeled hemispheres of *APL>shi^{ts1}* flies (right). $^{*}P < 0.05$, $^{**}P < 0.01$, $^{***}P < 0.001$, unpaired Welch *t*-test or repeated-measures ANOVA with Geisser-Greenhouse correction and Holm-Sidak multiple comparisons test as appropriate (lines connecting dots indicate repeated measures); *APL>shi^{ts1}* labeled condition in **c**, Friedman test with Dunn's multiple comparisons test. See **Supplementary Table 1** for full genotypes.

In imaging experiments on flies carrying *NP2631-GAL4*, *tubP-FRT-GAL80-FRT*, *GH146-Flp*, *mb247-LexA*, *lexAop-GCaMP3*, *UAS-mCherry* and *UAS-shi^{ts1}* transgenes ('*APL>shi^{ts1}*' flies; see **Supplementary Table 1**), hemispheres in which APL was unlabeled served as controls (**Fig. 4d** and **Supplementary Fig. 3a**,**e**,**i**). As before (**Fig. 1a**), odor-evoked responses in the Kenyon cells of control hemispheres were slightly reduced at 32 °C. This decrease may reflect the temperature dependence of Ca^{2+} binding and/or subsequent conformational changes in GCaMP3, cellular Ca^{2+} dynamics and/or Kenyon cell spike rates. In hemispheres where APL expressed dTRPA1, Kenyon cell odor responses were almost completely suppressed at 32 °C (**Fig. 4e** and **Supplementary Fig. 3b**,**f**,**i**), whereas in hemispheres where APL expressed shi^{ts1}, Kenyon cell responses were greatly boosted at the elevated temperature (**Fig. 4f** and **Supplementary Fig. 3c**,**g**,**i**). Acute (16–24 h) expression of functional TeTx in APL also increased Kenyon cell odor responses in comparison to the expression of inactive TeTx, whereas control hemispheres always showed wild-type odor responses (**Fig. 4g** and **Supplementary Fig. 3d**,**h**,**i**). These findings confirm that the APL neuron inhibits Kenyon cells, thus completing the feedback loop.

Inhibition keeps Kenyon cell responses sparse and distinct

Blocking feedback inhibition on Kenyon cells may not only enhance individual responses but also augment the responsive Kenyon cell population. Although odor-specific spatial patterns of activity are visible in optical sections of the mushroom body lobes, the tightly bundled axons make it impossible to resolve the processes of individual cells. Therefore, to estimate the sizes of the responsive Kenyon cell populations, we imaged Kenyon cell somata during stimulation with a panel of seven odors[18,40,41] and generated activity maps of the responsive pixels (**Fig. 5**). In control flies expressing only *mb247-LexA*–driven GCaMP3, and in APL-unlabeled hemispheres of *APL>shi^{ts1}* flies, raising the temperature did not alter the Kenyon cell odor response or slightly reduced it (**Fig. 5a**,**b**). In contrast, when either Kenyon cell or APL synaptic output was blocked by shi^{ts1} or TeTx, Kenyon cell

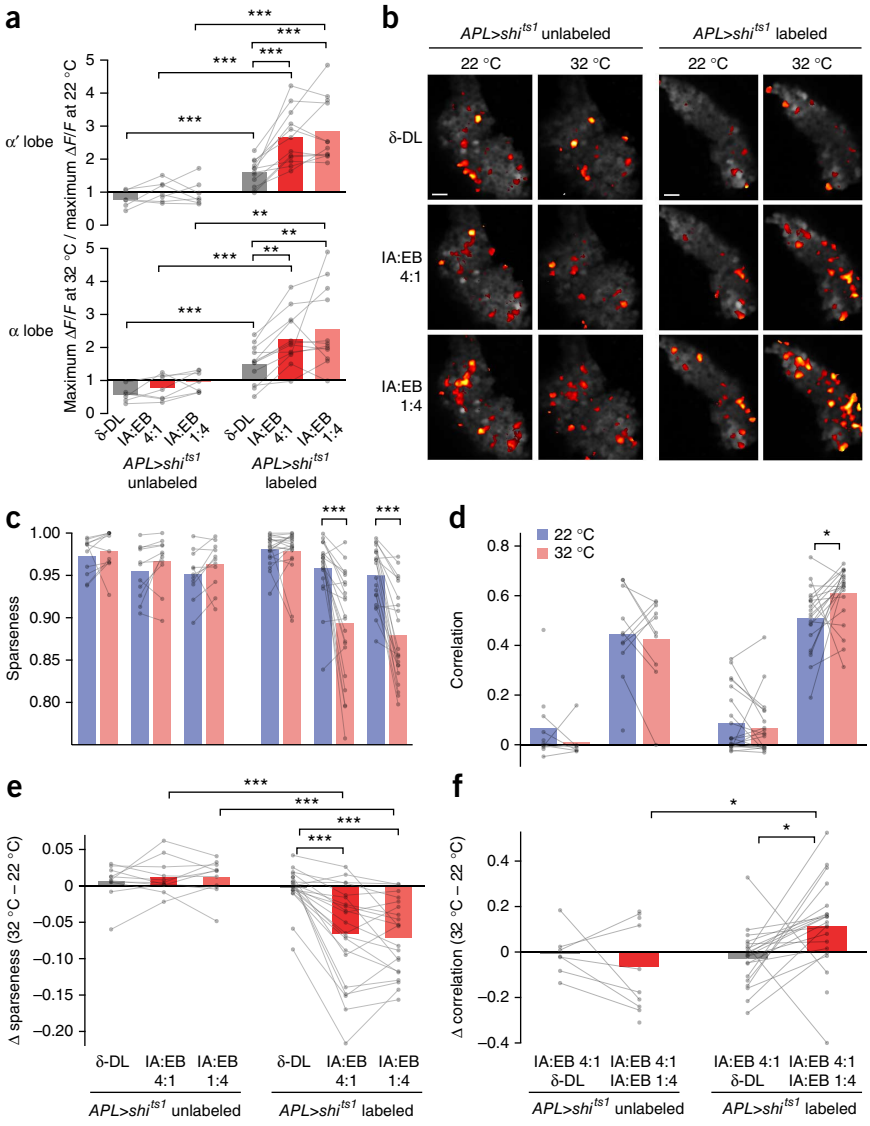

Figure 6 APL sparsens and decorrelates Kenyon cell responses. (**a**) Ratios of odor-evoked Ca^{2+} influx at 32 °C versus 22 °C in the α′ and α lobes, for δ-DL, IA:EB 1:4 and IA:EB 4:1, in hemispheres where the APL neuron was unlabeled ($n = 6$ or 7 [5]) or labeled ($n = 12$ [8]) with shi^{ts1}. n given as number of brain hemispheres [number of flies]. See **Supplementary Figure 5** for $\Delta F/F$ traces. $^{**}P < 0.01$, $^{***}P < 0.001$, Friedman test with Dunn's multiple comparisons test (top) or repeated-measures ANOVA with Geisser-Greenhouse correction and Holm-Sidak multiple comparisons test (bottom) for paired data; Bonferroni-corrected unpaired Welch t-test or Mann-Whitney U-test for unpaired data, as appropriate. (**b**) Activity maps of odor responses in Kenyon cell bodies. Scale bars, 10 µm; color scale as in **Figure 5**. (**c**) Population sparseness of activity maps in response to δ-DL, IA:EB 1:4 and IA:EB 4:1, at 22 °C (blue) and 32 °C (red). Blocking APL decreased sparseness only for IA:EB mixtures. (**d**) Correlations between activity maps for IA:EB 4:1 versus δ-DL and IA:EB 1:4, at 22 °C and 32 °C. Blocking APL increased correlations only between IA:EB mixtures. (**c**,**d**) $^{*}P = 0.013$, $^{***}P < 0.001$, Wilcoxon signed-rank test. (**e**) Temperature-dependent decrease in sparseness was greater for IA:EB mixtures than for δ-DL within APL-labeled hemispheres of $APL>shi^{ts1}$ flies and greater for IA:EB mixtures in APL-labeled than APL-unlabeled hemispheres of $APL>shi^{ts1}$ flies. $^{***}P < 0.001$, Mann-Whitney U-test (labeled versus unlabeled) or Friedman test with Dunn's multiple comparisons test (comparisons between odors). (**f**) Temperature-dependent increase in correlation was greater for IA:EB mixtures than for IA:EB 4:1 versus δ-DL within APL-labeled hemispheres of $APL>shi^{ts1}$ flies ($n = 20$ [13]) and greater for IA:EB mixtures in APL-labeled than APL-unlabeled hemispheres of $APL>shi^{ts1}$ flies ($n = 10$ [9]). $^{*}P = 0.020$, unpaired Welch t-test (between samples), $^{*}P = 0.022$, paired t-test (within samples).

odor responses became much broader and more similar (**Fig. 5a**,**b**). As with α lobe responses, removing Kenyon cells from the *OK107-GAL4* pattern with *mb247-LexA*-driven GAL80 eliminated the effect of *OK107-GAL4*-driven TeTx on sparseness and inter-odor similarity (**Supplementary Fig. 4**).

To quantify these effects, we measured the population sparseness[5] of the response patterns and determined correlations between the representations of different odors (see Online Methods). To avoid bias caused by manual cell identification, we applied sparseness and correlation metrics to unsegmented activity maps. In the best case, this method would replicate the results of manual cell identification (mathematically, sparseness and correlation remain the same if every element in each population is replicated an arbitrary number of times, as with each actual cell containing several pixels), and in the worst case it would merely add noise and thus be unlikely to create artificial effects.

In control flies, temperature did not alter the inter-odor correlations of activity maps (**Fig. 5c**) and marginally increased population sparseness (**Fig. 5d**), consistent with the previously observed decline in vertical lobe responses at the elevated temperature (**Fig. 4d**). In contrast, population sparseness decreased and inter-odor correlations increased when either Kenyon cell or APL synaptic output were blocked by shi^{ts1} or TeTx (**Fig. 5c–e**).

Inhibition enables learned discrimination of similar odors

Having established a mechanism that contributes to the sparseness of Kenyon cell odor responses, we were now in a position to test the function of sparse coding in odor-specific memory. We conjectured that broadening Kenyon cell odor responses by blocking APL would impair learned discrimination of similar, but not dissimilar, odors. Previous studies have manipulated inhibition in the periphery (the antennal lobe or olfactory bulb) and attributed impaired odor discrimination to a loss of synchrony or contrast among PN or mitral cell signals, respectively[42,43]. None of these studies has perturbed the sparseness of central odor representations in a directed manner.

Similar odor pairs for behavioral tests consisted of binary mixtures of isoamyl acetate (IA) and ethyl butyrate (EB) with component ratios of 1:4 and 4:1. To find an odor that would be well-separated from an IA:EB mixture, we consulted a database[40] of odor responses in olfactory receptor neurons (ORNs) and chose the odor that elicited the least overall ORN activity, δ-decalactone (δ-DL). Whereas IA and EB evoked a total of 2,030 and 1,860 spikes/s, respectively, in the

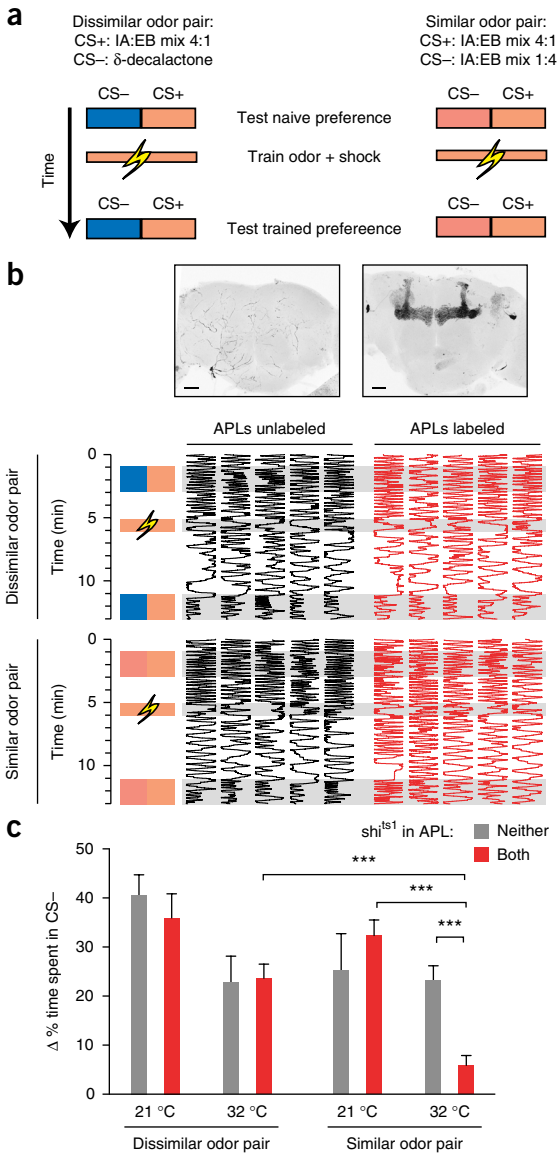

Figure 7 Feedback inhibition facilitates learned discrimination of similar, but not dissimilar, odors. (**a**) Training procedure. See text for details. (**b**) Top, maximum intensity projections of confocal image stacks showing example *APL>shi^{ts1},GFP* brains with neither or both APL neurons labeled. Scale bars, 50 µm. Bottom, individual odor preferences before and after training. Fly position in the chamber (horizontal dimension) is plotted against time (vertical dimension). (**c**) Performance of *APL>shi^{ts1},GFP* flies sorted according to whether neither or both APL neurons were labeled. Scores are plotted as change in the proportion of time spent in CS– after training. *n*, left to right, given as number of flies [number of experiments]: 23 [6], 26 [6], 16 [7], 44 [7], 18 [8], 55 [8], 32 [9], 51 [9]. ***$P < 0.001$, Kruskal-Wallis ANOVA with Holm-Bonferroni correction for *post hoc* tests, testing only pairs of data points with one variable changed (task, temperature or APL labeling). $P < 0.01$, three-way ANOVA for interaction of task, temperature and APL labeling. $P < 0.005$, two-way ANOVA for interaction of genotype and temperature for discrimination of similar odors. $P < 0.01$, two-way ANOVA for interaction of task and APL labeling at 32 °C. $P < 0.05$, two-way ANOVA for interaction of task and temperature for flies with both APL neurons labeled. Other two-way ANOVAs did not reveal significant interactions ($P > 0.11$). Error bars show s.e.m.

24 ORN types studied[40], δ-DL elicited only 286 spikes/s. Although ORN activity is transformed by the antennal lobe into PN activity with less variance in overall firing across odors[17,44], applying this transformation computationally[44] suggested that δ-DL elicits a low overall response compared to IA and EB at the PN level also (937, 1,238 and 1,310 spikes/s, respectively). In addition, while IA and EB generated correlated ORN and PN activity ($r = 0.47$ and 0.55, respectively), responses for δ-DL were uncorrelated to those for IA and EB (ORN, $r = 0.05$ and -0.07; PN, $r = -0.05$ and -0.04, respectively). Predicted PN responses to δ-DL were also sparser than those to IA or EB (population sparseness = 0.50 versus 0.42 and 0.35, respectively). Because modeled PN inputs representing δ-DL were naturally sparse and uncorrelated with those of IA and EB, we surmised that there would still be little overlap between Kenyon cell representations of δ-DL and an IA:EB mixture even with APL blocked.

To verify that this was the case, we imaged Kenyon cell responses to δ-DL, IA:EB 1:4 and IA:EB 4:1. For all three odors, as in **Figure 3**, blocking APL increased Kenyon cell responses in the α and α′ lobes (**Supplementary Fig. 5**). The increase was greater for the IA:EB mixtures than for δ-DL (**Fig. 6a**), supporting the idea that inhibitory feedback is driven by overall Kenyon cell activity (**Fig. 2**). Similarly, blocking APL broadened the responses of Kenyon cell somata to the IA:EB mixtures, but not to δ-DL (**Fig. 6b**). Quantitatively, raising the temperature did not affect sparseness or correlations for any of the three odors in hemispheres where APL was unlabeled. In hemispheres where the APL neuron expressed shi^{ts1}, raising the temperature did not affect the sparseness of δ-DL responses or δ-DL versus IA:EB 4:1 correlations, but it did decrease the sparseness of responses to IA:EB mixtures and increase their correlations (**Fig. 6c–f**). Blocking APL synaptic output thus compromises sparse coding and interferes with the decorrelation of Kenyon cell responses to IA:EB mixtures, which have relatively broad PN inputs, but not to δ-DL, which has relatively sparse PN inputs.

To test whether the broadening of Kenyon cell odor representations would impair learned odor discrimination, we used an individual-fly variant[27] of the classical T-maze task[26]. The ability to quantify individual behavior was essential for this analysis, as the stochastic nature of our genetic manipulation required that the performance of each of 694 flies bearing *NP2631-GAL4*, *tubP-FRT-GAL80-FRT*, *GH146-Flp*, *UAS-shi^{ts1}* and *UAS-CD8-GFP* transgenes be related to the occurrence of recombination events in APL. To determine whether recombination had taken place in both, one or neither of these neurons (see **Fig. 4a–c**), we dissected each fly after the behavioral measurements to see which APL neurons expressed GFP and, therefore, shi^{ts1}. Flies with both APL neurons labeled constituted the experimental group and flies with neither APL neuron labeled served as controls. All experimental flies thus had the same genotype aside from the stochastic excision of *GAL80* and subsequent expression of shi^{ts1} in the two APL neurons.

We measured odor discrimination in single-fly chambers that were perfused from each direction with clean or odor-infused air, so that the amount of time spent on each side provided a readout of preference[27]. Flies were first presented with a choice between two odors, one on each side, to benchmark their naive preferences, then with one odor paired with electric shock (CS+) and, after 5 min, with another choice between the original two odors. Anticipating that the behavioral effects of blocking APL might be subtle, we tried to make the learned discrimination more difficult by not presenting the unreinforced odor (CS–) during training, taking into account previous data showing that discrimination of two similar odors is more difficult[45] and performance on the classical T-maze is lower[26] when the unreinforced odor (CS–) is not encountered during training. Learning was measured as the difference in the proportion of time spent on the side with the

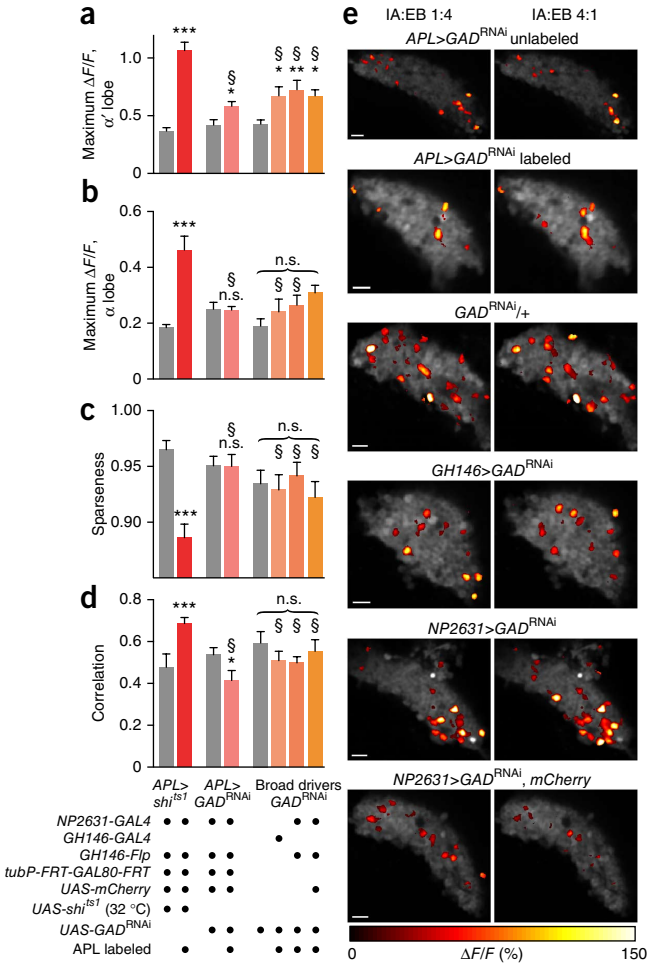

Figure 8 Partial effect of APL-specific RNAi of GABA biosynthesis. (**a**–**d**) See grid at bottom for full genotypes. (**a**,**b**) α′ (**a**) and α lobe (**b**) responses to IA:EB mixtures (averages of responses to 1:4 and 4:1). *n*, left to right, given as number of brain hemispheres [number of flies]: 7 [5], 12 [8], 11 [10], 15 [12], 7, 6, 6, 6. (**c**,**d**) Population sparseness (**c**) and correlations (**d**) of cell body responses to IA:EB mixtures (averages of responses to 1:4 and 4:1). *n*, left to right, given as number of brain hemispheres [number of flies]: 11 [9] (10 [9] in **d**), 21 [14], 11 [10], 15 [12], 10, 10, 6, 6. (**e**) Sample activity maps of cell body responses analyzed in **c**,**d**. Compare to **Figure 6b**. Scale bars, 10 μm. $*P < 0.05$, $**P < 0.01$, $***P < 0.001$ significant difference between colored bars and relevant controls (gray bars), by unpaired Welch *t*-test for *APL>shi*^{ts1} and *APL>GAD*^{RNAi} (Mann-Whitney *U*-test for *APL>shi*^{ts1} in **d**) and by one-way ANOVA and Dunnett's multiple comparisons test for *GH146-GAL4* and *NP2631-GAL4* driving *GAD*^{RNAi}. §$P < 0.05$ significant difference between effects of *GAD*^{RNAi} and *APL>shi*^{ts1} by two-way ANOVA (*P*, left to right: **a**: < 0.0001, 0.002, 0.006, 0.001; **b**: < 0.0001, 0.018, 0.028; **c**: 0.002, 0.008, 0.0007, 0.024; **d**: 0.0004, 0.003, 0.0038, 0.02). n.s., $P > 0.11$, one-way ANOVA or unpaired Welch *t*-test. Error bars, s.e.m.

unpunished odor (the CS–) before and after training. For learned discrimination of dissimilar odors, the CS+ was IA:EB 4:1 and the CS– was δ-DL, while for learned discrimination of similar odors, the CS+ was IA:EB 4:1 and the CS– was IA:EB 1:4 (**Fig. 7a**,**b**). Average untrained preferences between CS+ and CS– were close to 50:50 and did not vary significantly across groups (average untrained time in CS+ was between 47% and 53%; $P = 0.14$, Kruskal-Wallis ANOVA).

We predicted that blocking APL synaptic output would not prevent learned discrimination of δ-DL and IA:EB 4:1 because it did not increase the correlation between the Kenyon cell representations of these odors or decrease the sparseness of the δ-DL representation (**Fig. 6d**). Indeed, on this task, flies with both APL neurons labeled with shi^{ts1} performed the same as flies with neither APL neuron labeled, at both 21 °C and 32 °C (**Fig. 7b**,**c**). Although performance was lower overall at 32 °C, the lack of interaction between temperature and APL labeling shows that this effect was unrelated to shi^{ts1}-mediated APL blockade (two-way ANOVA: no interaction, $P = 0.53$; main effect of temperature, $P < 0.001$). Similarly, blocking APL synaptic output did not significantly affect learned discrimination of the dissimilar odors 3-octanol (OCT) and 4-methylcyclohexanol (MCH) (**Supplementary Fig. 6a**; two-way ANOVA: no interaction, $P = 0.82$; main effect of temperature, $P = 0.01$). We conclude that blocking APL does not impair olfactory associative learning *per se*, at least at the timescale of 5-min memory.

In contrast, when flies had to discriminate IA:EB 1:4 from IA:EB 4:1, odors whose Kenyon cell representations became less sparse and more correlated when APL was blocked (**Fig. 6**), animals with both APL neurons labeled with shi^{ts1} were impaired in comparison to animals with neither APL neuron labeled, at 32 °C but not at 21 °C (**Fig. 7b**,**c**; two-way ANOVA, significant interaction between temperature and APL labeling, $P = 0.0012$). Flies with only one APL neuron labeled showed a marginal, but not statistically significant, impairment in discriminating IA:EB 1:4 and IA:EB 4:1 (**Supplementary Fig. 6b**; $P = 0.16$, 0.80 for left and right APL neuron labeled versus neither neuron labeled at 32 °C). A three-way ANOVA revealed a significant interaction between odor pair similarity, temperature and shi^{ts1} expression in APL ($P = 0.009$). Together, these results suggest that sparse coding in Kenyon cells improves learned odor discrimination by reducing overlap between the representations of similar odors.

Partial effect of APL-specific RNAi of GABA biosynthesis

Because the APL neuron is GABAergic, interference with GABA biosynthesis might cause similar effects to blocking synaptic output. Indeed, RNAi-mediated knockdown of GAD expression in APL, using *GH146-GAL4*, has been reported to increase Kenyon cell odor responses[16] and improve learning[34] of MCH and OCT. However, in preliminary experiments, we did not observe any impairment in learned discrimination of IA:EB 1:4 versus IA:EB 4:1 in flies expressing *GAD*^{RNAi} driven by *GH146-GAL4* (data not shown).

We suspected that knockdown of GABA signaling might be incomplete. RNAi rarely results in a complete knockout of the target gene[46], and compensating homeostasis can partially negate the effect of a knockdown. Negative feedback systems such as the Kenyon cell–APL circuit may be especially robust to partial perturbations, as any reduced inhibition of Kenyon cells would increase the excitatory drive to APL, which might offset the partial depletion of GABA. *GH146>GAD*^{RNAi} and *NP2631>GAD*^{RNAi} reduce GABA immunoreactivity in the APL neuron[34,38], but as immunohistochemistry is not necessarily linear, the degree of knockdown is unclear. Therefore, we directly compared the effects of *GAD*^{RNAi} and shi^{ts1} in APL on Kenyon cell responses to IA:EB 1:4 and IA:EB 4:1.

We expressed *GAD*^{RNAi} specifically in the APL neuron using our intersectional strategy. As compared to APL-unlabeled hemispheres, Kenyon cell odor responses in APL-labeled hemispheres were modestly higher in the α′ lobe (**Fig. 8a**), but not the α lobe (**Fig. 8b**). In both lobes, the effect of *APL>GAD*^{RNAi} was significantly smaller than the effect of *APL>shi*^{ts1} (two-way ANOVA, $P < 0.0001$). In Kenyon cell somata, *APL>GAD*^{RNAi} had no effect on population sparseness and slightly decreased the correlation between responses to IA:EB 1:4 and IA:EB 4:1 (**Fig. 8c**–**e**).

We also compared this modest effect with the effects of the previously published[16,34,38] manipulations *GH146>GAD*^{RNAi} and *NP2631>GAD*^{RNAi}. To ensure that the coexpression of *UAS-mCherry* with *GAD*^{RNAi} in our APL-specific labeling strategy did not lessen the efficacy of *GAD*^{RNAi} by titrating GAL4, we also tested *NP2631>GAD*^{RNAi}, *UAS-mCherry* flies. All three manipulations slightly increased α′, but not α, lobe responses to IA:EB 1:4 and IA:EB 4:1 relative to control *GAD*^{RNAi}/+ flies, but had no effect on population sparseness or correlation. Again, the effects of *GAD*^{RNAi} were significantly smaller than the effect of *APL>shi*^{ts1} (**Fig. 8**). We saw similar results in vertical lobe odor responses to ethyl acetate and cell body responses to the panel of odors used in **Figure 5** (**Supplementary Fig. 7**). There was a modest, though not statistically significant ($P = 0.26$), increase in mean inter-odor correlation with *GH146>GAD*^{RNAi} and *NP2631>GAD*^{RNAi}, which was smaller than the increase in correlation seen with *APL>shi*^{ts1}. Across all conditions, we thus found that APL-specific blockade of synaptic output with shi^{ts1} was a more stringent perturbation than *GH146>GAD*^{RNAi} or *NP2631>GAD*^{RNAi}.

DISCUSSION

Theoretical work has long predicted that sparse coding increases memory capacity by reducing overlap between representations of similar stimuli[1–4,13], but experimental evidence tying sparse coding to behavior has been lacking. We present here the first such evidence, to our knowledge, by showing (i) that the APL neuron sparsens and decorrelates Kenyon cell responses and (ii) that disrupting sparse, decorrelated odor coding by blocking APL impairs learned discrimination of similar, but not dissimilar, odors.

In *Drosophila*, associative memories are thought to be written to Kenyon cell output synapses when a Kenyon cell is activated by odor at the same time as a reward or punishment induces release of neuromodulators such as dopamine onto the Kenyon cell[19,27]. The input odor, in the form of its PN activity pattern, specifies the memory address (that is, the Kenyon cells whose synapses are to be modified) and induces the retrieval of the memory by activating the Kenyon cells whose synapses were modified during training[19,27]. If odor coding is too broad (that is, too many Kenyon cells are activated by each odor), the likelihood is increased of unwanted overlap, in which an irrelevant odor activates enough Kenyon cells storing the memory that the conditioned response is inappropriately triggered. Our results support this model by showing that, when the loss of APL feedback decreased sparseness (**Figs. 5** and **6**), learned discrimination of similar odors was impaired (**Fig. 7**). Sparse coding was important only insofar as it decorrelated odor representations: even if the sparseness of the CS+ representation was reduced, learned discrimination was unaffected if the correlation between the CS+ and CS− representations remained low, as with the dissimilar odors IA:EB 4:1 and δ-DL (**Figs. 6** and **7**). Consistent with this conclusion, the greater the overlap between the Kenyon cell representations of two odors, the greater the difficulty wild-type flies have in learning to discriminate the two odors[41]. This model therefore generates the testable prediction that blocking APL synaptic output will differentially affect learned discrimination of other similar and dissimilar odor pairs.

It remains formally possible that the defect in learned odor discrimination is caused by effects of blocking APL synaptic output that are unrelated to sparse coding. The only way to prove definitively that sparseness is the mediating factor would be to induce memory formation and retrieval by activating pairs of arbitrary subpopulations of Kenyon cells with varying degrees of sparseness and similarity, an experiment beyond current technological capabilities. That said, the manipulation used here—acutely blocking the output of a single neuron, which innervates only the mushroom body—is remarkably specific. In addition, blocking APL synaptic output did not affect learning of a dissimilar odor pair, arguing against a general learning defect. The most plausible explanation of the data is therefore that the effect of APL on learned discrimination occurs via this neuron's role in enforcing sparse coding.

Our results provide new perspectives on previous behavioral findings concerning APL. Learned discrimination of the dissimilar odors MCH and OCT at 3 h after training involves both gap junctions between the dorsal paired medial (DPM) neuron and the APL neuron[47] and APL synaptic output during consolidation[35]. Inhibition by APL was suggested to maintain the odor-specificity of memory during consolidation in a mechanism involving recurrent activity between DPM and α′β′ neurons[35]. The proposed APL–DPM–α′β′ loop is unlikely to play a role in our experiments, because DPM output is not required for short-term memory of most odors[48]. However, our results are nevertheless connected: the importance of the sparsening effect of APL for discrimination of similar odors in short-term memory, shown here, may extend to learned discrimination of dissimilar odors at longer time scales, when recurrent activity loops may spiral out of control without feedback inhibition.

It has also been found that reducing GABA synthesis in APL by RNAi increases Kenyon cell odor responses and can improve learning[16,34]. The apparent discrepancy can be explained by the partial effect on Kenyon cell odor responses of *APL>GAD*^{RNAi} relative to *APL>shi*^{ts1} (**Fig. 8**): a modest increase in Kenyon cell activity may improve memory retrieval by increasing Kenyon cell output while not overly compromising sparseness or discrimination, whereas the large increase in Kenyon cell activity by *APL>shi*^{ts1} overwhelms the Kenyon cell population's ability to represent similar odors separately, thereby impairing discrimination. Consistent with this notion, *APL>GAD*^{RNAi} manipulations do not affect the sparseness of, or correlation between, Kenyon cell representations of MCH and OCT, the odors used in the previous studies showing improved learning in *GH146>GAD*^{RNAi} flies (**Supplementary Fig. 8**). *GAD*^{RNAi} in APL can also prevent olfactory reversal learning[37], most likely because the initial memory is too strong. Finally, APL responses to the CS+ decline after aversive training[34], possibly as a result of synaptic depression between APL and Kenyon cells that respond to the CS+. However, this change in APL responses to the CS+ is most likely dispensable for short-term memory because flies with both APL neurons blocked can still learn to discriminate dissimilar odors (**Fig. 7**).

Why is APL feedback inhibition required to maintain sparse coding? Kenyon cells respond sparsely in part because they act as coincidence detectors, requiring inputs from multiple PNs to spike[8,18]. However, the remarkably robust sparse coding in Kenyon cells[12] has been difficult to explain by computational modeling using only thresholded summation. Sparse coding in modeled Kenyon cells lies in a narrow, unstable band between silence and indiscriminate firing[15], and thresholded summation of simulated PN odor responses results in frequent detection failures[14]. Only adding global inhibition provides the modeled Kenyon cells with the flexibility to respond sparsely to a wide range of odors[14,15]. Indeed, locust GGN odor responses increase with stimulus intensity[15,49], suggesting that feedback inhibition scales with input to stabilize sparseness. Consistent with this scenario, we found that the small difference in Kenyon cell sparseness in control conditions between the narrow odor δ-DL and the broad IA:EB mixtures was much larger when we blocked APL feedback (**Fig. 6**). Computational studies have modeled inhibitory regulation of Kenyon cell sparseness using both feedback[15] and feedforward[14,50] inhibition, but feedback

appears to be the main mechanism[49], perhaps because the fragility of sparse coding requires the error-canceling logic of feedback. The presence of both recurrent inhibition and sparse odor coding in the mammalian olfactory cortex[10,11,20] suggests that inhibitory cortical interneurons may play a similar role to the *Drosophila* APL neuron in olfactory discrimination.

METHODS

Methods and any associated references are available in the online version of the paper.

Note: Any Supplementary Information and Source Data files are available in the online version of the paper.

ACKNOWLEDGMENTS

We thank M. Parnas and S. DasGupta for discussions; Y. Tan, R. Roorda, C. Talbot and J. Beevers for technical assistance; L. Looger (Janelia Farm Research Campus) for a plasmid encoding GCaMP3; and S. Goodwin (University of Oxford), C.-H. Lee (US National Institutes of Health), L. Luo (Stanford University), K. Scott (University of California, Berkeley), S. Waddell (University of Oxford), the Bloomington Stock Center, the Kyoto *Drosophila* Genetic Resource Center and the Vienna *Drosophila* RNAi Center for fly strains. This work was supported by grants from the Wellcome Trust (090309/Z/09/Z; G.M.), the Gatsby Charitable Foundation (G.M.), the UK Medical Research Council (G0700888; G.M.), the US National Institutes of Health (R01DA030601; G.M.), the Oxford Martin School (G.M.), the Howard Hughes Medical Institute (T.L.), a Sir Henry Wellcome Postdoctoral Fellowship (089021/Z/09/Z; A.C.L.) and a Wellcome Trust OXION studentship (A.M.B.).

AUTHOR CONTRIBUTIONS

A.C.L. and G.M. designed the study, analyzed the results and wrote the paper. A.C.L. performed all behavioral and imaging experiments. A.M.B. assisted with behavioral experiments and dissections and A.d.C. with dissections. T.L. provided *lexAop-shi^{ts1}* and *mb247-LexA* flies.

COMPETING FINANCIAL INTERESTS

The authors declare no competing financial interests.

1. Kanerva, P. *Sparse Distributed Memory* (MIT Press, 1988).
2. Marr, D. A theory of cerebellar cortex. *J. Physiol.* (*Lond.*) **202**, 437–470 (1969).
3. Albus, J.S. A theory of cerebellar function. *Math. Biosci.* **10**, 25–61 (1971).
4. Treves, A. & Rolls, E.T. What determines the capacity of autoassociative memories in the brain? *Network* **2**, 371–397 (1991).
5. Vinje, W.E. & Gallant, J.L. Sparse coding and decorrelation in primary visual cortex during natural vision. *Science* **287**, 1273–1276 (2000).
6. Hromádka, T., Deweese, M.R. & Zador, A.M. Sparse representation of sounds in the unanesthetized auditory cortex. *PLoS Biol.* **6**, e16 (2008).
7. Crochet, S., Poulet, J.F.A., Kremer, Y. & Petersen, C.C.H. Synaptic mechanisms underlying sparse coding of active touch. *Neuron* **69**, 1160–1175 (2011).
8. Perez-Orive, J. *et al.* Oscillations and sparsening of odor representations in the mushroom body. *Science* **297**, 359–365 (2002).
9. Ito, I., Ong, R.C.-Y., Raman, B. & Stopfer, M. Sparse odor representation and olfactory learning. *Nat. Neurosci.* **11**, 1177–1184 (2008).
10. Stettler, D.D. & Axel, R. Representations of odor in the piriform cortex. *Neuron* **63**, 854–864 (2009).
11. Poo, C. & Isaacson, J.S. Odor representations in olfactory cortex: 'sparse' coding, global inhibition, and oscillations. *Neuron* **62**, 850–861 (2009).
12. Honegger, K.S., Campbell, R.A.A. & Turner, G.C. Cellular-resolution population imaging reveals robust sparse coding in the *Drosophila* mushroom body. *J. Neurosci.* **31**, 11772–11785 (2011).
13. Jortner, R.A., Farivar, S.S. & Laurent, G. A simple connectivity scheme for sparse coding in an olfactory system. *J. Neurosci.* **27**, 1659–1669 (2007).
14. Luo, S.X., Axel, R. & Abbott, L.F. Generating sparse and selective third-order responses in the olfactory system of the fly. *Proc. Natl. Acad. Sci. USA* **107**, 10713–10718 (2010).
15. Papadopoulou, M., Cassenaer, S., Nowotny, T. & Laurent, G. Normalization for sparse encoding of odors by a wide-field interneuron. *Science* **332**, 721–725 (2011).
16. Lei, Z., Chen, K., Li, H., Liu, H. & Guo, A. The GABA system regulates the sparse coding of odors in the mushroom bodies of *Drosophila*. *Biochem. Biophys. Res. Commun.* **436**, 35–40 (2013).
17. Bhandawat, V., Olsen, S.R., Gouwens, N.W., Schlief, M.L. & Wilson, R.I. Sensory processing in the *Drosophila* antennal lobe increases reliability and separability of ensemble odor representations. *Nat. Neurosci.* **10**, 1474–1482 (2007).
18. Turner, G.C., Bazhenov, M. & Laurent, G. Olfactory representations by *Drosophila* mushroom body neurons. *J. Neurophysiol.* **99**, 734–746 (2008).
19. Heisenberg, M. Mushroom body memoir: from maps to models. *Nat. Rev. Neurosci.* **4**, 266–275 (2003).
20. Franks, K.M. *et al.* Recurrent circuitry dynamically shapes the activation of piriform cortex. *Neuron* **72**, 49–56 (2011).
21. Kapfer, C., Glickfeld, L.L., Atallah, B.V. & Scanziani, M. Supralinear increase of recurrent inhibition during sparse activity in the somatosensory cortex. *Nat. Neurosci.* **10**, 743–753 (2007).
22. Ng, M. *et al.* Transmission of olfactory information between three populations of neurons in the antennal lobe of the fly. *Neuron* **36**, 463–474 (2002).
23. Kitamoto, T. Conditional modification of behavior in *Drosophila* by targeted expression of a temperature-sensitive shibire allele in defined neurons. *J. Neurobiol.* **47**, 81–92 (2001).
24. Lima, S.Q. & Miesenböck, G. Remote control of behavior through genetically targeted photostimulation of neurons. *Cell* **121**, 141–152 (2005).
25. Hamada, F.N. *et al.* An internal thermal sensor controlling temperature preference in *Drosophila*. *Nature* **454**, 217–220 (2008).
26. Tully, T. & Quinn, W.G. Classical conditioning and retention in normal and mutant *Drosophila melanogaster*. *J. Comp. Physiol. A* **157**, 263–277 (1985).
27. Claridge-Chang, A. *et al.* Writing memories with light-addressable reinforcement circuitry. *Cell* **139**, 405–415 (2009).
28. Thum, A.S. *et al.* Differential potencies of effector genes in adult *Drosophila*. *J. Comp. Neurol.* **498**, 194–203 (2006).
29. Sweeney, S.T., Broadie, K., Keane, J., Niemann, H. & O'Kane, C.J. Targeted expression of tetanus toxin light chain in *Drosophila* specifically eliminates synaptic transmission and causes behavioral defects. *Neuron* **14**, 341–351 (1995).
30. Aso, Y. *et al.* The mushroom body of adult *Drosophila* characterized by GAL4 drivers. *J. Neurogenet.* **23**, 156–172 (2009).
31. Hu, A., Zhang, W. & Wang, Z. Functional feedback from mushroom bodies to antennal lobes in the *Drosophila* olfactory pathway. *Proc. Natl. Acad. Sci. USA* **107**, 10262–10267 (2010).
32. Markopoulos, F., Rokni, D., Gire, D.H. & Murthy, V.N. Functional properties of cortical feedback projections to the olfactory bulb. *Neuron* **76**, 1175–1188 (2012).
33. Boyd, A.M., Sturgill, J.F., Poo, C. & Isaacson, J.S. Cortical feedback control of olfactory bulb circuits. *Neuron* **76**, 1161–1174 (2012).
34. Liu, X. & Davis, R.L. The GABAergic anterior paired lateral neuron suppresses and is suppressed by olfactory learning. *Nat. Neurosci.* **12**, 53–59 (2009).
35. Pitman, J.L. *et al.* A pair of inhibitory neurons are required to sustain labile memory in the *Drosophila* mushroom body. *Curr. Biol.* **21**, 855–861 (2011).
36. Liu, X., Krause, W.C. & Davis, R.L. $GABA_A$ receptor RDL inhibits *Drosophila* olfactory associative learning. *Neuron* **56**, 1090–1102 (2007).
37. Wu, Y., Ren, Q., Li, H. & Guo, A. The GABAergic anterior paired lateral neurons facilitate olfactory reversal learning in *Drosophila*. *Learn. Mem.* **19**, 478–486 (2012).
38. Ren, Q., Li, H., Wu, Y., Ren, J. & Guo, A. A GABAergic inhibitory neural circuit regulates visual reversal learning in *Drosophila*. *J. Neurosci.* **32**, 11524–11538 (2012).
39. Wilson, R.I. & Laurent, G. Role of GABAergic inhibition in shaping odor-evoked spatiotemporal patterns in the *Drosophila* antennal lobe. *J. Neurosci.* **25**, 9069–9079 (2005).
40. Hallem, E.A. & Carlson, J.R. Coding of odors by a receptor repertoire. *Cell* **125**, 143–160 (2006).
41. Campbell, R.A.A. *et al.* Imaging a population code for odor identity in the *Drosophila* mushroom body. *J. Neurosci.* **33**, 10568–10581 (2013).
42. Stopfer, M., Bhagavan, S., Smith, B.H. & Laurent, G. Impaired odour discrimination on desynchronization of odour-encoding neural assemblies. *Nature* **390**, 70–74 (1997).
43. Abraham, N.M. *et al.* Synaptic inhibition in the olfactory bulb accelerates odor discrimination in mice. *Neuron* **65**, 399–411 (2010).
44. Olsen, S.R., Bhandawat, V. & Wilson, R.I. Divisive normalization in olfactory population codes. *Neuron* **66**, 287–299 (2010).
45. Mishra, D., Louis, M. & Gerber, B. Adaptive adjustment of the generalization-discrimination balance in larval *Drosophila*. *J. Neurogenet.* **24**, 168–175 (2010).
46. Dietzl, G. *et al.* A genome-wide transgenic RNAi library for conditional gene inactivation in *Drosophila*. *Nature* **448**, 151–156 (2007).
47. Wu, C.-L. *et al.* Heterotypic gap junctions between two neurons in the *Drosophila* brain are critical for memory. *Curr. Biol.* **21**, 848–854 (2011).
48. Keene, A.C. *et al.* Diverse odor-conditioned memories require uniquely timed dorsal paired medial neuron output. *Neuron* **44**, 521–533 (2004).
49. Gupta, N. & Stopfer, M. Functional analysis of a higher olfactory center, the lateral horn. *J. Neurosci.* **32**, 8138–8148 (2012).
50. Assisi, C., Stopfer, M., Laurent, G. & Bazhenov, M. Adaptive regulation of sparseness by feedforward inhibition. *Nat. Neurosci.* **10**, 1176–1184 (2007).

ONLINE METHODS

Fly strains. The following transgenic strains of *Drosophila melanogaster* were used: *UAS-shi^{ts1}* (refs. 23,51), *mb247-LexA::VP16* (ref. 35), *lexAop-GAL80* (ref. 52), *OK107-GAL4* (ref. 53), *tubP-GAL80^{ts}* (ref. 54), *UAS-TeTx* and *UAS-TeTx-inactive* (H233V, H237V)[29], *UAS-synapto-pHluorin* (refs. 22,55), *UAS-dTRPA1* (ref. 25), *lexAop-dTRPA1* (ref. 56), *lexAop-CD2::RFP* (ref. 57), *NP225-GAL4* (ref. 58) and *NP2631-GAL4* (Kyoto *Drosophila* Genetic Resource Center), *c739-GAL4* (ref. 30), *R35B12-GAL4* and *R64C08-GAL4* (ref. 59), *tubP-FRT-GAL80-FRT* (refs. 60,61), *GH146-Flp* (ref. 62), *mb247-dsRed* (ref. 63), *UAS-mCherry::CAAX* (ref. 64) and *UAS-CD8::GFP*. Expression cassettes encoding GCaMP3 (ref. 65) and shi^{ts1} fused to *UAS* or *lexAop* regulatory sequences were targeted to *attP2* and *attP16* landing sites or inserted randomly, respectively (Genetic Services, Inc.).

Flies were cultivated on cornmeal agar under a 12-h light/12-h dark cycle at 25 °C unless they expressed temperature-sensitive gene products (*shi^{ts1}*, *GAL80^{ts}*, *dTRPA1*); in these cases, the experimental animals and all relevant controls were grown at 18 °C. Flies carrying *tubP-GAL80^{ts}* were raised at 18 °C and placed at 31 °C for 16–24 h <1 d after eclosion. All experiments were performed on male and female flies aged 1–7 d.

Behavior. Learned odor discrimination was analyzed in clear polycarbonate chambers (length 50 mm, width 5 mm, height 1.3 mm) incorporating printed circuit boards (PCBs) with 1-mm electrodes and 1-mm electrode gaps as floors and ceilings[27]. Solid-state relays (Fairchild HSR312L) connected the PCBs to a 60-V source. For electric shock reinforcement, the relays were activated for 1.25 s at a repetition rate of 0.2 Hz during a 1-min odor presentation[27].

Flow-controlled (2.7 l/min; CMOSens PerformanceLine, Sensirion), filtered and humidified carrier air was mixed with flow-controlled odor streams (0.3 l/min) drawn through vials filled with 10^{-2} dilutions of odorant in mineral oil. IA:EB 1:4 and 4:1 were 2×10^{-3}:8×10^{-3} and vice versa. The air/odor streams were split among 20 chambers, yielding a flow rate of 0.15 l/min per half-chamber. A stack of 20 chambers was backlit by 940-nm LEDs (TSAL6100, Vishay) and imaged by a Stingray F080B CCD camera (Allied Vision Technologies) equipped with a Computar M1614 lens. The apparatus was operated in a temperature-controlled incubator (Sanyo MIR-154) maintained at 21 or 32 °C, as indicated. To impose a synaptic transmission block[23] with shi^{ts1}, experimental and control animals were transferred to the restrictive temperature of 32 °C for 15 min before the start of a behavioral experiment and maintained at the elevated temperature throughout. Flies were individually recovered into food vials and their brains were dissected to score recombination events in APL (see Structural imaging). Behavioral experiments were performed during the day (9 a.m.–8 p.m.).

A virtual instrument written in LabVIEW 2009 (National Instruments) extracted fly position data from video images and controlled the delivery of odors and electric shocks[27]. Experimental data were analyzed offline in MATLAB 2012a (MathWorks). The amount of time a fly spent in each half of the chamber was scored during the initial naive test and the final post-training test, and the learned discrimination was calculated as the difference in percentage time in CS– after and before training. Flies making fewer than two entries into the choice zone during odor presentation were excluded from analysis.

Functional imaging. Cuticle and trachea in a small window overlying the mushroom body were surgically removed, and the exposed brain was superfused with carbogenated solution (95% O_2, 5% CO_2) containing 5 mM TES, 103 mM NaCl, 3 mM KCl, 1.5 mM $CaCl_2$, 4 mM $MgCl_2$, 26 mM $NaHCO_3$, 1 mM NaH_2PO_4, 8 mM trehalose and 10 mM glucose, pH 7.3. Heating for shi^{ts1} and dTRPA1 experiments was provided by a TC-10 temperature controller (NPI) and an HPT-2 inline perfusion heater (ALA). For dTRPA1 experiments, the temperature at the fly was measured with a TS-200 miniature temperature sensor (NPI) and a USB-1208FS DAQ device (Measurement Computing) at 30 Hz; temperature traces were smoothed over 20 frames by a moving-average filter to remove digitization artifacts. For shi^{ts1} experiments, flies were held at 32 °C for at least 15 min and provided with 10–15 odor pulses before imaging to deplete the synaptic vesicle pool. Both hemispheres were imaged where possible in APL-specific labeling experiments with shi^{ts1}, dTRPA1, TeTx or *GAD^{RNAi}*, counting unlabeled hemispheres as controls; brains were dissected after each experiment to score recombination events in APL. Unresponsive or damaged brains were excluded from analysis.

Odors at 10^{-2} dilution were delivered[66] by switching mass-flow controlled air/odor streams (CMOSens PerformanceLine, Sensirion) with a custom-built solenoid valve system (The Lee Company). An odor tube ~5 mm in diameter was positioned ~1 cm from the fly's head. The flow rate at the fly was 0.5 l/min.

Fly brains were imaged using two-photon microscopy[22,66]. Fluorescence was excited with 140-fs pulses of light centered at 910 nm (Chameleon Ultra II, Coherent). The excitation laser was attenuated with the help of a Pockels cell (Conoptics 302RM) and coupled to the scan engine of a Movable Objective Microscope (Sutter Instruments) equipped with a Zeiss 20×, 1.0 NA W-Plan-Apochromat objective. Emitted photons were separated from excitation light by a series of dichromatic mirrors and dielectric and colored glass filters and detected by GaAsP photomultiplier tubes (Hamamatsu Photonics H10770PA-40 SEL). Photomultiplier currents were amplified (Laser Components HCA-4M-500K-C) and passed through a custom-designed integrator circuit to maximize the signal-to-noise ratio. The microscope was controlled through MPScope 2.0 via a PCI-6110 DAQ board (National Instruments).

Images were converted to Analyze format and motion-corrected by maximizing the pixel-by-pixel correlation between a reference frame and each frame in the time series. $\Delta F/F$ traces were calculated in ImageJ by subtracting background fluorescence and taking the average signal in the region of interest over time, subtracting and then dividing by the average pre-stimulus signal, using manually drawn regions of interest for the background and brain structure of interest. Traces were smoothed by a moving average over five frames and linearly interpolated to a frame time of 0.09 s in Igor Pro to allow averaging of movies with different frame rates. To match $\Delta F/F$ with temperature for dTRPA1 experiments, the smoothed temperature trace was linearly interpolated to the frame rate of the $\Delta F/F$ trace.

Activity maps were generated in MATLAB after smoothing with a Gaussian filter and background subtraction. A baseline fluorescence image was calculated as the average over the pre-stimulus interval. Frames in which the brain moved in the axial direction were automatically discarded by correlating each frame to the baseline image and discarding it if the correlation fell below a threshold value, which was manually selected for each brain by noting the constant high correlation value when the brain was stationary and sudden drops in correlation when the brain moved. For this motion elimination, pixel values were capped to prevent bona fide odor responses from causing changes in correlation values. For each pixel, the difference between mean intensity during the stimulus and the mean baseline fluorescence (ΔF) was calculated. If ΔF of a pixel was less than twice the s.d. (σ) of the intensity of that pixel during the pre-stimulus interval, the pixel was considered unresponsive. (A 2σ threshold corresponds to the top ~5% of a normal distribution.) Activity maps were smoothed with a Gaussian filter for display purposes, but not for further similarity and sparseness analyses.

Inter-odor similarity was calculated in MATLAB by first aligning the activity maps of each odor response by maximizing the inter-odor correlations of baseline fluorescence and then converting image matrices of the activity maps of each odor response into linear vectors and calculating the Pearson correlation coefficients between each 'odor vector'. A threshold for baseline fluorescence was applied as a mask to the activity map to exclude pixels with no baseline GCaMP3 signal. Population sparseness was calculated for activity maps using the equation[5,67]

$$S_P = \frac{1}{1-\frac{1}{N}}\left(1-\frac{\left(\sum_{i=1}^{N}\frac{r_i}{N}\right)^2}{\sum_{i=1}^{N}\frac{r_i^2}{N}}\right)$$

For rare maps where no pixel had a $\Delta F/F$ greater than the 2σ threshold, sparseness was set to 1.0 and correlations involving that map were not calculated.

Statistical analysis. Statistical analyses were performed in Prism 6 (GraphPad) and R 2.14.2 (http://www.r-project.org/). Data were tested for normality and

homogeneity of variances before being analyzed with parametric (*t*-test, ANOVA) or nonparametric tests (Mann-Whitney, Friedman, Kruskal-Wallis), as appropriate. Random assignment to experimental groups was not used. In general, no statistical tests were done to predetermine sample size. However, where a conclusion relied on the absence of a significant effect (**Fig. 1d** and **Supplementary Fig. 6a**), a power analysis was performed to confirm that the sample size was sufficient to detect an effect of the expected size. The experimenter was blind to which APL neurons were labeled before postexperimental dissection (**Figs. 4–8**) but not otherwise.

Structural imaging. Brains were dissected and fixed in 4% (wt/vol) paraformaldehyde in PBS (1.86 mM NaH_2PO_4, 8.41 mM Na_2HPO_4, 175 mM NaCl) for 20–60 min at room temperature under vacuum. Samples were washed three times for 10 min each with PBS containing 0.1% (vol/vol) Triton X-100 (PBT) and twice in PBS before mounting in Vectashield (Vector Labs). Images were collected on a Leica TCS SP5 confocal microscope and processed in Fiji.

APL expression of shi^{ts1}, dTRPA1 and GAD^{RNAi} was scored by widefield imaging of mCherry (for functional imaging experiments) or GFP (for behavioral experiments) in unfixed brains mounted in PBS. APL expression of TeTx and TeTx-inactive was detected by immunostainings using rabbit anti-TeTx antibody (POL 016, Statens Serum Institut, 1:100) and goat anti-rabbit Alexa 546 conjugate (Jackson ImmunoResearch, 1:800). Primary and secondary antisera were applied for 2 d in PBT at 4 °C. The dsRed driven by the *3XP3* promoter in the *GH146-Flp* insertion[62] was not expressed in the mushroom body and therefore did not interfere with the detection of mCherry or TeTx in APL.

51. Pfeiffer, B.D., Truman, J.W. & Rubin, G.M. Using translational enhancers to increase transgene expression in *Drosophila*. *Proc. Natl. Acad. Sci. USA* **109**, 6626–6631 (2012).
52. Thistle, R., Cameron, P., Ghorayshi, A., Dennison, L. & Scott, K. Contact chemoreceptors mediate male-male repulsion and male-female attraction during *Drosophila* courtship. *Cell* **149**, 1140–1151 (2012).
53. Connolly, J.B. *et al.* Associative learning disrupted by impaired Gs signaling in *Drosophila* mushroom bodies. *Science* **274**, 2104–2107 (1996).
54. McGuire, S.E., Le, P.T., Osborn, A.J., Matsumoto, K. & Davis, R.L. Spatiotemporal rescue of memory dysfunction in *Drosophila*. *Science* **302**, 1765–1768 (2003).
55. Miesenböck, G., De Angelis, D.A. & Rothman, J.E. Visualizing secretion and synaptic transmission with pH-sensitive green fluorescent proteins. *Nature* **394**, 192–195 (1998).
56. Burke, C.J. *et al.* Layered reward signalling through octopamine and dopamine in *Drosophila*. *Nature* **492**, 433–437 (2012).
57. Awasaki, T., Huang, Y., O'Connor, M.B. & Lee, T. Glia instruct developmental neuronal remodeling through TGF-β signaling. *Nat. Neurosci.* **14**, 821–823 (2011).
58. Thum, A.S., Jenett, A., Ito, K., Heisenberg, M. & Tanimoto, H. Multiple memory traces for olfactory reward learning in *Drosophila*. *J. Neurosci.* **27**, 11132–11138 (2007).
59. Jenett, A. *et al.* A GAL4-driver line resource for *Drosophila* neurobiology. *Cell Reports* **2**, 991–1001 (2012).
60. Gao, S. *et al.* The neural substrate of spectral preference in *Drosophila*. *Neuron* **60**, 328–342 (2008).
61. Gordon, M.D. & Scott, K. Motor control in a *Drosophila* taste circuit. *Neuron* **61**, 373–384 (2009).
62. Hong, W. *et al.* Leucine-rich repeat transmembrane proteins instruct discrete dendrite targeting in an olfactory map. *Nat. Neurosci.* **12**, 1542–1550 (2009).
63. Riemensperger, T., Völler, T., Stock, P., Buchner, E. & Fiala, A. Punishment prediction by dopaminergic neurons in *Drosophila*. *Curr. Biol.* **15**, 1953–1960 (2005).
64. Kakihara, K., Shinmyozu, K., Kato, K., Wada, H. & Hayashi, S. Conversion of plasma membrane topology during epithelial tube connection requires Arf-like 3 small GTPase in *Drosophila*. *Mech. Dev.* **125**, 325–336 (2008).
65. Tian, L. *et al.* Imaging neural activity in worms, flies and mice with improved GCaMP calcium indicators. *Nat. Methods* **6**, 875–881 (2009).
66. Shang, Y., Claridge-Chang, A., Sjulson, L., Pypaert, M. & Miesenböck, G. Excitatory local circuits and their implications for olfactory processing in the fly antennal lobe. *Cell* **128**, 601–612 (2007).
67. Willmore, B. & Tolhurst, D.J. Characterizing the sparseness of neural codes. *Network* **12**, 255–270 (2001).